ARTICLE Open Access

Quantum entanglement network enabled by a state-multiplexing quantum light source

Yun-Ru Fan[1,2,3], Yue Luo[1,3], Kai Guo[4]✉, Jin-Peng Wu[1,3], Hong Zeng[1,3], Guang-Wei Deng[1,3,5], You Wang[1,6], Hai-Zhi Song[1,6], Zhen Wang[7], Li-Xing You[7], Guang-Can Guo[1,2,3,8] and Qiang Zhou[1,2,3,8]✉

Abstract

A fully connected quantum network with a wavelength division multiplexing architecture plays an increasingly pivotal role in quantum information technology. With such architecture, an entanglement-based network has been demonstrated in which an entangled photon-pair source distributes quantum entanglement resources to many users. Despite these remarkable advances, the scalability of the architecture could be constrained by the finite spectrum resource, where $\mathcal{O}(N^2)$ wavelength channels are needed to connect N users, thus impeding further progress in real-world scenarios. Here, we propose a scheme for the wavelength division multiplexing entanglement-based network using a state-multiplexing quantum light source. With a dual-pump configuration, the feasibility of our approach is demonstrated by generating state-multiplexing photon pairs at multiple wavelength channels with a silicon nitride microring resonator chip. In our demonstration, we establish a fully connected graph between four users with six wavelength channels—saving half of which without sacrificing functionality and performance of the secure communication. A total asymptotic secure key rate of 1946.9 bps is obtained by performing the BBM92 protocol with the distributed state. The network topology of our method has great potential for developing a scalable quantum network with significantly minimized infrastructure requirements.

Introduction

Entanglement-based quantum network, in which the information is encoded on and measured from entangled photons, facilitates the development of quantum computation, quantum metrology, and quantum communication[1–5]. The quantum network has undergone extensive exploration, encompassing different types of configurations, such as point-to-point[6], trusted-node[7–16], point-to-multipoint[17–19], and fully connected network[20–27]. Among these, the fully connected network, i.e., each user of the network simultaneously sharing quantum correlations and exchanging quantum information or quantum secure key with every other user, has emerged as one of the most versatile and robust architectures with the advancement of multiplexing technology in degrees of freedom in wavelength, space, and time. Harnessing progresses in wavelength division multiplexing (WDM), a four-user entanglement-based wavelength-multiplexed quantum network has been realized by using a polarization-entangled photon pair with twelve wavelength channels[20]. In such a network, $N \times (N-1)$ wavelength channels are needed to accommodate N users, which is constrained to only a few due to the finite spectrum resource of the photon-pair source[28–36]. To expand the network with available resources, a quadratic improvement in wavelength saving has been achieved with the establishment of an eight-user metropolitan network featuring 16 wavelength channels—with eight beamsplitters for passively temporal multiplexing at the expense of decreasing the rate of information[21]. To further achieve a scalable and reconfigurable quantum network, flex-grid entanglement distributions have been implemented by employing multiplexing techniques based on wavelength selective switch technology, which enables the reconfigurability of a quantum network with ever-increasing complexity and service demands[25–27].

Correspondence: Kai Guo (guokai07203@hotmail.com) or Qiang Zhou (zhouqiang@uestc.edu.cn)
[1]Institute of Fundamental and Frontier Sciences, University of Electronic Science and Technology of China, Chengdu 611731, China
[2]Center for Quantum Internet, Tianfu Jiangxi Laboratory, Chengdu 641419, China
Full list of author information is available at the end of the article

Despite these great promises, the fully connected quantum network has been demonstrated based on such a quantum light source that a quantum state is prepared on a wavelength. To leverage the finite wavelength resources, we propose a novel scheme of the quantum network based on a state-multiplexing quantum light source. This approach employs two lasers to pump a third-order nonlinear optical device, facilitating three spontaneous four-wave mixing (SFWM) processes simultaneously—one non-degenerate[37–43] and two degenerate processes[44–46]. Therefore, a wavelength overlap could be created, enabling photons at one wavelength channel to be correlated with photons at the other three wavelength channels, and thus reducing the wavelength resources needed for a fully connected network.

In this work, we developed a state-multiplexing photon-pair source by using two lasers to pump a fiber-pigtailed silicon nitride microring resonator (MRR) chip with a free spectral range (FSR) of 200 GHz. The source enables a fully connected graph between four users with six wavelength channels, which saves half of the wavelength channels compared with the previous result[20]. Our result shows that such a framework could allow simultaneous and secure connections with a total asymptotic secure key rate of 1946.9 bps by performing the BBM92 protocol. The network topology exhibits the potential to establish a scalable and reconfigurable quantum network, which reduces the infrastructure requirement, thus paving the way for developing a large-scale quantum secure network in the future.

Results

Network scheme with state-multiplexing quantum light source

As shown in Fig. 1a, state-multiplexing photon pairs are generated by pumping a nonlinear optical device with a laser module emitting light at two wavelengths. Taking the third-order nonlinear optical device as an example, the degenerate and non-degenerate SFWM processes could occur at the same time, i.e., correlated/entangled photons are generated with the pump configurations of $2\omega_{p1}$, $2\omega_{p2}$, and $\omega_{p1}+\omega_{p2}$, respectively. For instance, we denote the two wavelengths of the pump laser module as 0 and 10, whereby the photon pairs are entangled when the sum of their numerical labels equals 0, 20, or 10, corresponding to the degenerate or non-degenerate SFWM processes, respectively. For the wavelength at ω_2 (labeled as 2), the photons could be correlated/entangled with those at another three wavelengths ω_1, ω_3, and ω_4—labeled as −2, 8, and 18. Thus, three quantum states are

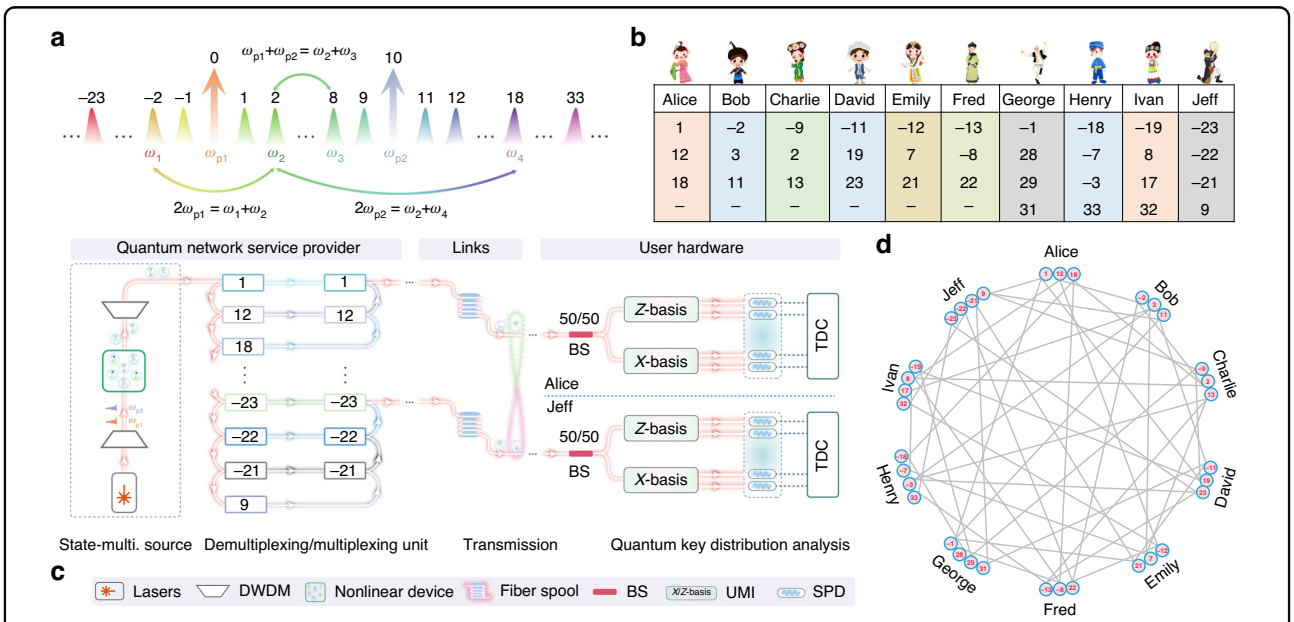

Fig. 1 Schematic of quantum network with a state-multiplexing quantum light source. a State-multiplexing quantum light source with dual-pump configuration, i.e., $2\omega_{p1}$, $2\omega_{p2}$, and $\omega_{p1}+\omega_{p2}$, respectively. Photons at the wavelength of ω_2 can be correlated/entangled with photons at another three wavelengths—ω_1, ω_3, and ω_4, i.e., three quantum states are prepared on a common wavelength by multiplexing. **b** Wavelength allocation of quantum network for ten users. With pump photons labeled as 0 and 10, two users can establish connections by photon pair whose labels sum up to 0, 10, or 20, respectively. **c** Physical layer of the quantum network. It consists of the quantum network service provider (QNSP), links, and user hardware, in which quantum states from QNSP are distributed to each user via fiber links. Each user is equipped with a beam splitter and two interferometers to perform the random choice of measurement basis between Z (0 or π) and X ($\pi/2$ or $3\pi/2$). **d** Communication layer of the quantum network for ten users. With the scheme, ten users are fully connected with 34 wavelength channels, which saves 56 wavelength channels compared to the previous scheme[20]

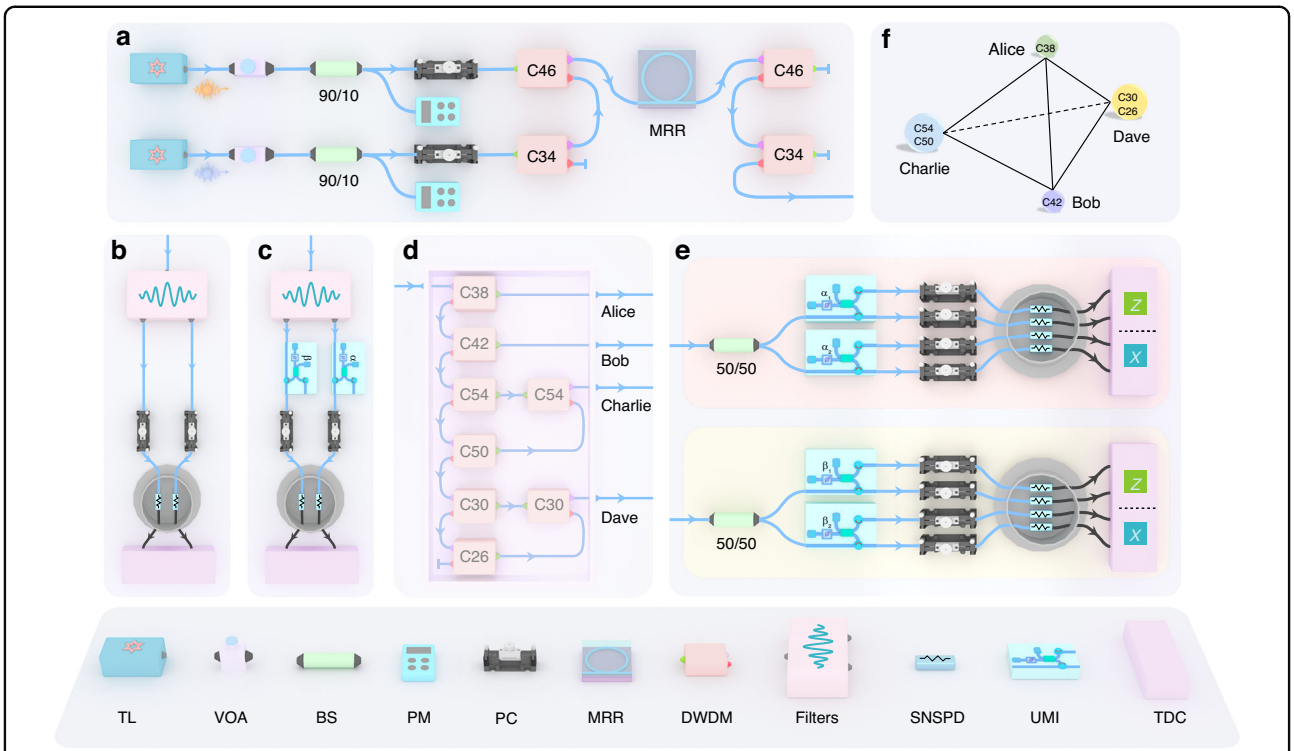

Fig. 2 Schematic diagram of experimental setups. a Generation of correlated photon pairs with dual pumps. **b** Correlation properties. **c** Energy-time entanglement with Franson interference. **d** Demultiplexing/multiplexing unit for the four-node quantum network with six wavelength channels. **e** Measurement setup for quantum key distribution using the BBM92 protocol. **f** Communication layer and wavelength allocation. Note that the sketch of the PC is adopted from Thorlabs. TL Tunable laser, VOA Variable optical attenuator, BS Beam splitter, PM Power meter, PC Polarization controller, MRR Microring resonator, DWDM Dense wavelength division multiplexer, SNSPD Superconducting nanowire single-photon detector, UMI Unbalanced Michelson interferometer, TDC Time-to-digital converter

multiplexed on a common wavelength with our method. Leveraging such a state-multiplexing quantum light source, a user who occupies one wavelength resource can connect with the other three users.

Physical and communication layers of the quantum network featuring a state-multiplexing quantum light source are illustrated in Fig. 1c, d, respectively. The physical layer contains a central quantum network service provider (QNSP), fiber links, and user hardware. As shown in Fig. 1c, the QNSP includes the state-multiplexing quantum light source and the demultiplexing/multiplexing unit, while the user hardware consists of a beam splitter (BS), two unbalanced Michelson interferometers (UMIs), and four single-photon detectors (SPDs). Photons incident on the BS and UMIs, where they are measured in the Z basis (0 or π) or the X basis ($\pi/2$ or $3\pi/2$), thus enabling the measurement in the diagonal/antidiagonal phase basis. The communication layer of the network facilitates a fully connected graph, enabling entanglement distribution, quantum information exchange, and secure communication between all pairs of users. We conceptually refer to the ten users of our network as Alice (A), Bob (B), Charlie (C), Dave (D), Emily (E), Fred (F), George (G), Henry (H), Ivan (I), and Jeff (J). Every user within the ten-node network receives wavelength channels identified by numerical labels. The wavelength allocation is shown in Fig. 1b. Benefiting from the state-multiplexing quantum light source, this scenario necessitates 34 wavelength channels for the ten-node network, a considerable reduction compared to 90 wavelength channels suggested in the previous result[20].

State-multiplexing quantum light source with dual pumps

The generation and characterization of quantum state-multiplexing photon pairs with dual pumps is illustrated in Fig. 2. A fiber-pigtailed silicon nitride microring resonator chip is utilized with an FSR of ~200 GHz and a quality factor of ~10^6 [47]. See more details in Methods and Supplemental Material Note 1. As shown in Fig. 2a, two independent continuous-wave tunable lasers at the wavelengths of 1550.12 nm and 1540.56 nm without phase-stable with each other are used to generate photon pairs, which are multiplexed by using dense wavelength division multiplexers (DWDMs) with 200-GHz-spacing at the ITU channels of C34 and C46. In our experiments, the power of the two pump lasers is set to be equal in order to

balance the efficiencies of the degenerate and non-degenerate type-0 SFWM processes, ensuring the optimized performance of the state-multiplexing quantum light source[40,48]. Quantum state-multiplexing photon pairs are generated in the resonator. After the pump rejection, signal and idler photons are selected by DWDMs and detected and recorded by superconducting nanowire single-photon detectors (SNSPDs) and time-to-digital converter (TDC), respectively, as shown in Fig. 2b.

To characterize the quantum correlation property of generated photons, we select the ITU channel C38 as the common wavelength, photons from which are correlated/entangled with those from the ITU channels C30, C42, and C54. The single side count rates at C30, C42, and C54 with different pump power are measured as shown in Fig. 3a. The error bars of the count rate are obtained by the Poissonian photon-counting statistic. The difference in the rates comes from the different quality factors and transmission losses of these channels. See more details in Supplemental Material Note 2. The coincidence count rates and coincidence-to-accidental ratios (CARs) are given in Fig. 3b, c. In Fig. 3b, the inset shows the coincidence histograms for the correlated photon pairs between C30&C38, C42&C38, and C54&C38 at a pump power of 1 mW, respectively. It is worth noting that the coincidence count rates and CARs in the non-degenerate case are higher than those in the degenerate case because of the different efficiency between degenerate and non-degenerate SFWM processes[37,42,43,49].

The property of energy-time entanglement of the state-multiplexing quantum light source is verified by the Franson interference[50,51] by using two identical UMIs with an additional phase difference of α or β as shown in Fig. 2c. Note that the interferometers are stabled by the proportional-integral-derivative (PID) feedback control with reference light. See more details in Supplemental Material Note 3. The measured interference curves of C30&C38, C38&C42, and C38&C54 are shown in Fig. 3d–f the phases of $\beta = \pi/2$ and $\pi/4$. Circles are experimental results, while the lines are the fitting curves with a 1000-time Monte Carlo method. For $\beta = \pi/4$, the raw visibility is obtained as 87.1 ± 0.5%, 98.2 ± 0.2%, and 90.4 ± 0.6% without subtracting the accidental coincidence counts. The single side count rates of photons at C30, C42, and C54 keep constant at ~108 kHz, ~141 kHz, and ~57 kHz, respectively, which indicates that there is no single-photon interference in the measurement. The quantum correlation and entanglement properties of other photon pairs are characterized by measuring the coincidence events between signal and idler photons at different wavelength channels, as illustrated in Fig. 3g and Table 1. Note that the correlation and entanglement

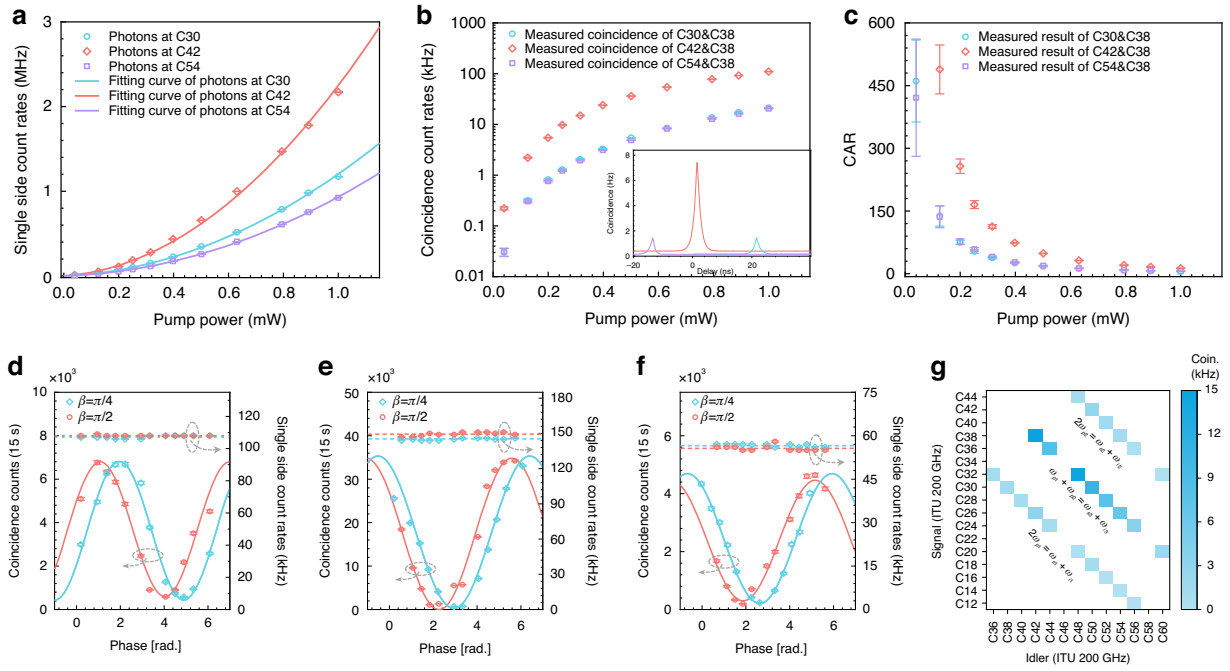

Fig. 3 Experimental results of the state-multiplexing quantum light source with dual pumps. a Single side count rates of photons at different levels of pump power at the wavelength of C30, C42, and C54, which is correlated/entangled with the photons at C38—the state-multiplexing state. **b** Coincidence count rates and **c** CAR of photon pairs for C30&C38, C38&C42, and C38&C54. The inset of **b** gives the coincidence histograms for the three correlated photon pairs. **d**–**f** Results of Franson interference for C30&C38, C38&C42, and C38&C54, respectively. **g** Coincidence count rates of 24-wavelength-paired photon pairs for degenerate and non-degenerate SFWM processes at pump powers at 0.32 mW

properties at C22 and C58 are not shown in the results due to the classical light generated from the stimulated four-wave mixing process[52,53].

Quantum key distribution

With the developed state-multiplexing quantum light source, we demonstrate the feasibility of the energy-time entanglement-based quantum key distribution network between four users with six wavelength channels. As shown in Fig. 2f, Alice (A), Bob (B), Charlie (C), and Dave (D) are connected by photon pairs at C38, C42, C54/C50, and C30/C26, respectively. Figure 2d shows the details of the demultiplexing/multiplexing unit, in which six DWDMs are used for demultiplexing while two DWDMs are used for multiplexing, respectively. See more details in Tables S1–S4 in Supplemental Material for losses of the different schemes. We analyze the quantum bit error rate (QBER) and the asymptotic secure key rate (SKR) between two different users by performing the BBM92 protocol[54] as shown in Fig. 2e. The results indicate that the performance between Alice and Bob is the best because of the high-efficiency photon generation and low-noise wavelength configuration, while the performance between Bob and Dave is the worst as photons at C30 are considered noises in this case.

Table 1 Experimental results of the Franson interference for energy-time entanglement generated from the state-multiplexing quantum light source through degenerate and non-degenerate type-0 SFWM processes

SFWM process	ITU channels	Visibility	ITU channels	Visibility
Degenerate	C32&C36	91.1 ± 0.4%	C30&C38	87.1 ± 0.5%
	C28&C40	93.9 ± 0.5%	C26&C42	83.9 ± 0.5%
	C24&C44	99.8 ± 0.3%	C20&C48	83.4 ± 0.9%
	C18&C50	85.4 ± 0.6%	C16&C52	87.0 ± 1.6%
	C14&C54	83.4 ± 1.1%	C12&C56	85.4 ± 1.9%
	C44&C48	90.8 ± 0.4%	C42&C50	91.9 ± 0.4%
	C40&C52	83.7 ± 0.5%	C38&C54	90.4 ± 0.4%
	C36&C56	90.3 ± 0.3%	C32&C60	88.1 ± 0.8%
Non-degenerate	C36&C44	94.9 ± 0.2%	C38&C42	98.2 ± 0.2%
	C32&C48	96.2 ± 0.3%	C30&C50	94.3 ± 0.2%
	C28&C52	98.4 ± 0.2%	C26&C54	95.7 ± 0.1%
	C24&C56	99.9 ± 0.3%	C20&C60	91.4 ± 0.5%

The secure key rate is calculated by $SKR = N_{sift} \times [1 - f(\delta_b) \times H_2(\delta_b) - H_2(\delta_p)]$[22,55–58] where N_{sift} is the sifted key rate, $f(\delta_b)$ characterizes the efficiency of error correction with respect to Shannon's noisy coding theorem, the value of which is set to 1.2 in our calculation, $\delta_{b,p}$ is the bit or the phase error rate, and $H_2(\delta_{b,p})$ is the binary entropy function as $H_2(\delta_{b,p}) = -\delta_{b,p}\log_2(\delta_{b,p}) - (1 - \delta_{b,p})\log_2(1 - \delta_{b,p})$, respectively. In the experiments, N_{sift} and QBER increase as the pump power, leading to a trade-off between N_{sift} and QBER for a high-performance quantum network. To obtain the optimal pump power, we measure the visibility, N_{sift}, QBER, and SKR of B&D at different pump powers, as shown in Fig. 4a, b[55]. At a pump power of 0.4 mW, the visibility and QBER approach the limit for successful key generation, which is 80.9% and 9.5% with $f(\delta_b) = 1.2$ respectively, as illustrated by the blue dashed lines in Fig. 4a, b. See more details of the calculation in Supplemental Material Note 7. Further increasing the pump power would lead to failure of key generation between users B and D. Therefore, we set the pump powers as 0.4 mW and analyze the properties between different combinations of users. The coincidence histogram results of A&B, A&C, A&D, B&C, B&D, and C&D are shown in Fig. 4c. The results of quantum key distribution are listed in Table 2. A total SKR of 1946.9 bps among four users is obtained, which is higher than that by using a single pump scheme. See more details

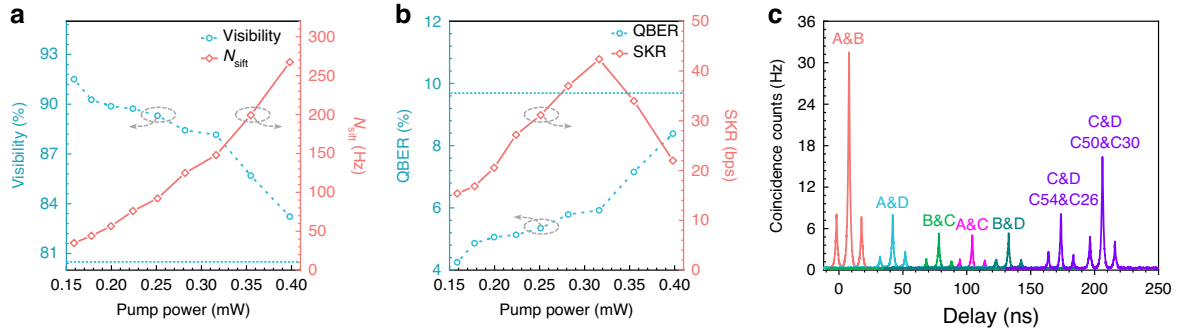

Fig. 4 Experimental results of quantum key distribution with the developed state-multiplexing quantum light source. a, **b** shows the visibility, N_{sift}, QBER, and SKR of B&D at different pump power levels. **c** Histograms between A&B, A&C, A&D, B&C, B&D, and C&D. Users C and D share two sets of correlated wavelengths with two sets of correlation peaks

Table 2 Results of the QBER and SKR between A&B, A&C, A&D, B&C, B&D, and C&D

Users	ITU channel	N_{sift} (Hz)	Visibility	QBER	SKR (bps)
A&B	C38&C42	1613.9	97.1%	1.4%	1230.6
A&C	C38&C54	260.0	84.4%	7.8%	34.2
A&D	C38&C30	405.6	87.1%	6.5%	97.6
B&C	C42&C50	268.2	84.9%	7.6%	39.9
B&D	C42&C26	267.4	83.2%	8.4%	22.9
C&D	C50&C30	585.0	93.2%	3.4%	454.6
C&D	C54&C26	460.0	84.8%	7.6%	67.1
Total					1946.9

in Table S5 in Supplemental Material for the performance comparison. The results suggest that our scheme not only preserves the functionality of secure communication but also conserves wavelength channels and enhances performance. It is noted that C and D are connected by two entangled photon pairs—C50&C30 and C54&C26.

Discussion

To further improve the SKR of the quantum network, we can utilize a quantum light source with a smaller coincidence window or coherence time[59], which can be realized by utilizing dual-Mach-Zehner microring device[60] and dual-microring device with parity-time symmetry[61]. See more details for the theoretical analysis of SKR in Supplemental Material Note 7. One may argue that the QBER and, hence, the SKR are limited by the inevitable noise of our scheme. For instance, in our demonstration, three states are prepared on one wavelength by multiplexing, with only one state being used while the other two are considered noise. However, this is also the case in the previous scheme, where the quantum state in one wavelength channel is contaminated by other wavelength channels without demultiplexing or frequency-resolved detection at the user node. The QBER and SKR in the quantum network with state-multiplexing quantum light source are not only determined by the generation properties of the photon pairs, but also determined by the configuration of the network topology. For instance, in our demonstration, users C and D occupy two wavelength channels, i.e., C54/C50 and C30/C26, respectively. Therefore, the correlation properties of C38&C54 and C38&C30 are also influenced by photons in the wavelength channels of C50 and C26. One can balance the generation efficiencies of degenerate and non-degenerate processes and configure the arrangement of DWDMs among channels, and can also apply the flexible grid idea to dynamically balance the SKR [25–27].

The long-term goal of a full-fledged quantum internet requires a quantum communication network that supports the connection among as many users as possible using minimal wavelength channels. As the number of users increases, the advantages of our scheme become increasingly pronounced. The pump configuration can be customized and dynamically adjusted to tailor specific requirements. For instance, employing three or more pump lasers would further extend the spectrum range in which entangled two-photon states can be generated in the device. More multiplexed states would be prepared on a wavelength, thus increasing the scalability of the quantum network. To further configure the entanglement distribution network, one can adjust the powers and wavelengths of pump lasers to dynamically manipulate its connections. It is worth noting that with more pumps, more challenges and complexities in noise filtering and channel assignment will be introduced. Especially wavelength channels could be occupied by light generated from stimulated FWM processes. One could utilize the type-II SFWM process to develop the state-multiplexing quantum light source, in which the stimulated FWM can be further suppressed[40,48]. Besides, the bandwidth of quantum light source can be further extended by dispersion engineering of the SiN microring with inverse-design approach[62]. Alternatively, nonlinear optical devices fabricated with different third-order nonlinear optical materials, such as GaN[36], AlGaAs[63–65], can also be utilized for developing broadband state-multiplexing quantum light sources. Furthermore, the number of wavelength channels can be increased by reducing the FSR of the microring [28,31].

In summary, we have successfully implemented an energy-time entanglement-based quantum key distribution network using a state-multiplexing quantum light source for the first time, which confirms the enhanced feasibility and scalability of the proposed network architecture. Our state-multiplexing scheme can also be applied to quantum networks with various entanglement resources such as polarization entanglement and time-bin entanglement. Besides, combining with the time-sharing[24], BS multiplexing[21], and flex-gride[25–27], our scheme enables the realization of larger-scale quantum network.

Materials and methods

Details of silicon nitride microring resonator chip

Silicon nitride (Si_3N_4) microring resonator chip can offer enhanced nonlinear effects by leveraging their resonant nature thanks to its ultralow optical loss and tailorable dispersion[34]. In our experiments, we demonstrate a quantum network using a microring resonator with a Si_3N_4 chip. The width-height cross-section of our microring resonators is designed as 1.8 μm × 0.8 μm for the anomalous dispersion. The gap between the waveguide and the ring is 0.35 μm with over-coupling for high-performance quantum light generation and emission. The microring chip is packaged by single-mode I/O fibers with

an insertion loss of 3.2 dB, which is realized by using microlenses for precise mode matching and optical collimators for efficient coupling. The image of the fiber-pigtailed chip with thermal stability management is shown in Fig. S1a. The transmission spectra of the microring from 1533 nm to 1558 nm are shown in Fig. S1b. Figure S1c, d gives the details at C46 and C34 with a quality factor of 1.29×10^6 and 1.22×10^6, respectively.

Experimental setup

The experimental setup for the generation of photon pairs is shown in Fig. 2a in the main text. Two continuous-wave tunable lasers (Toptica CTL 1550) at 1550.12 nm (ITU Channel C34) and 1540.56 nm (ITU Channel C46) are utilized. The power is adjusted by a variable optical attenuator (VOA) and is monitored by a 90:10 BS and a power meter. The polarization controller is used to control the polarization to align the TE00 mode of the waveguide. To suppress the sideband noise of the laser and the Raman photons generated in the fiber, two high-isolation (>120 dB) DWDMs at C46 and C34 are employed before the microring chip. Then the pump light at wavelengths of C34 and C46 are multiplexed and injected into the chip. At the output of the chip, the residual pump laser is rejected by two DWDMs with an isolation of >50 dB.

Thermal stability

To maintain the thermal stability of the microring resonator, a thermoelectric cooler, and a thermistor are packaged at the bottom of the device, both of which are connected to a temperature controller with the PID method. The temperature stability can be maintained within 0.001 °C, which ensures the thermal stability of the microring resonator.

Frequency stability

To keep the pump lasers at the resonant wavelengths of the microring resonator, a wavelength meter (WS8-10, HighFinesse) with PID option is used to stabilize the wavelengths of the two narrow linewidth lasers (DLC CTL 1550, Toptica). The measured frequency shifts of the two lasers are shown in the inset of Fig. S1a, b, which is within 1 MHz for both channels. Compared to the linewidth of ~200 MHz for the resonance, the pump laser can be stably tuned into the microring resonator. At the resonant wavelengths, the stability of our setups is further monitored by measuring the powers of the two pump lasers after passing through the microring resonator. As shown in Fig. S8c, the results indicate that conditions are almost the same during the measurement.

Acknowledgements
This work was supported by Sichuan Science and Technology Program (Nos. 2022YFSY0061, 2022YFSY0062, 2022YFSY0063, 2023YFSY0062, 2023YFSY0058, 2023NSFSC0048), the National Natural Science Foundation of China (Nos. 62475039, 62405046, 92365106, 62105371), Innovation Program for Quantum Science and Technology (No. 2021ZD0300701).

Author details
[1]Institute of Fundamental and Frontier Sciences, University of Electronic Science and Technology of China, Chengdu 611731, China. [2]Center for Quantum Internet, Tianfu Jiangxi Laboratory, Chengdu 641419, China. [3]Key Laboratory of Quantum Physics and Photonic Quantum Information, Ministry of Education, University of Electronic Science and Technology of China, Chengdu 611731, China. [4]Institute of Systems Engineering, AMS, Beijing 100141, China. [5]Hefei National Laboratory, University of Science and Technology of China, Hefei 230088, China. [6]Southwest Institute of Technical Physics, Chengdu 610041, China. [7]National Key Laboratory of Materials for Integrated Circuits, Shanghai Institute of Microsystem and Information Technology, Chinese Academy of Sciences, Shanghai 200050, China. [8]CAS Key Laboratory of Quantum Information, University of Science and Technology of China, Hefei 230026, China

Author contributions
Q.Z. conceived and supervised the project. Y.-R.F. mainly carried out the experiment and collected the experimental data with the help of other authors. Z.W. and L.-X.Y. developed and maintained the SNSPDs used in the experiment. Y.-R.F., K.G., and Q.Z. analyzed the data and wrote the manuscript with inputs from all other authors. All authors have given approval for the final version of the manuscript.

Data availability
All data needed to evaluate the conclusions in the paper are present in the paper and/or the Supplementary Information. Additional data related to this paper may be requested from the authors.

Conflict of interest
The authors declare no competing interests.

Supplementary information The online version contains supplementary material available at https://doi.org/10.1038/s41377-025-01805-1.

Received: 17 November 2024 Revised: 18 February 2025 Accepted: 3 March 2025
Published online: 12 May 2025

References

1. Kimble, H. J. The quantum internet. *Nature* **453**, 1023–1030 (2008).
2. Simon, C. Towards a global quantum network. *Nat. Photonics* **11**, 678–680 (2017).
3. Wehner, S., Elkouss, D. & Hanson, R. Quantum internet: a vision for the road ahead. *Science* **362**, eaam9288 (2018).
4. Wei, S. H. et al. Towards real-world quantum networks: a review. *Laser Photonics Rev.* **16**, 2100219 (2022).
5. Qi, Z. T. et al. A 15-user quantum secure direct communication network. *Light Sci. Appl.* **10**, 183 (2021).
6. Scarani, V. et al. The security of practical quantum key distribution. *Rev. Mod. Phys.* **81**, 1301–1350 (2009).
7. Elliott, C. Building the quantum network. *N. J. Phys.* **4**, 46 (2002).
8. Peev, M. et al. The SECOQC quantum key distribution network in Vienna. *N. J. Phys.* **11**, 075001 (2009).
9. Xu, F. X. et al. Field experiment on a robust hierarchical metropolitan quantum cryptography network. *Chin. Sci. Bull.* **54**, 2991–2997 (2009).
10. Stucki, D. et al. Long-term performance of the SwissQuantum quantum key distribution network in a field environment. *N. J. Phys.* **13**, 123001 (2011).
11. Sasaki, M. et al. Field test of quantum key distribution in the Tokyo QKD network. *Opt. Express* **19**, 10387–10409 (2011).
12. Wang, S. et al. Field and long-term demonstration of a wide area quantum key distribution network. *Opt. Express* **22**, 21739–21756 (2014).
13. Mao, Y. Q. et al. Integrating quantum key distribution with classical communications in backbone fiber network. *Opt. Express* **26**, 6010–6020 (2018).
14. Dynes, J. F. et al. Cambridge quantum network. *npj Quantum Inf.* **5**, 101 (2019).

15. Evans, P. G. et al. Trusted node QKD at an electrical utility. *IEEE Access* **9**, 105220–105229 (2021).
16. Chen, Y. A. et al. An integrated space-to-ground quantum communication network over 4600 kilometres. *Nature* **589**, 214–219 (2021).
17. Townsend, P. D. Quantum cryptography on multiuser optical fibre networks. *Nature* **385**, 47–49 (1997).
18. Choi, I., Young, R. J. & Townsend, P. D. Quantum information to the home. *N. J. Phys.* **13**, 063039 (2011).
19. Fröhlich, B. et al. A quantum access network. *Nature* **501**, 69–72 (2013).
20. Wengerowsky, S. et al. An entanglement-based wavelength-multiplexed quantum communication network. *Nature* **564**, 225–228 (2018).
21. Joshi, S. K. et al. A trusted node–free eight-user metropolitan quantum communication network. *Sci. Adv.* **6**, eaba0959 (2020).
22. Wen, W. J. et al. Realizing an entanglement-based multiuser quantum network with integrated photonics. *Phys. Rev. Appl.* **18**, 024059 (2022).
23. Liu, X. et al. 40-user fully connected entanglement-based quantum key distribution network without trusted node. *PhotoniX* **3**, 2 (2022).
24. Liu, J. Y. et al. Reconfigurable entanglement distribution network based on pump management of a spontaneous four-wave mixing source. *Sci. Adv.* **10**, eado9822 (2024).
25. Alshowkan, M. et al. Reconfigurable quantum local area network over deployed fiber. *PRX Quantum* **2**, 040304 (2021).
26. Appas, F. et al. Flexible entanglement-distribution network with an AlGaAs chip for secure communications. *npj Quantum Inf.* **7**, 118 (2021).
27. Alshowkan, M. et al. Advanced architectures for high-performance quantum networking. *J. Opt. Commun. Netw.* **14**, 493–499 (2022).
28. Imany, P. et al. 50-GHz-spaced comb of high-dimensional frequency-bin entangled photons from an on-chip silicon nitride microresonator. *Opt. Express* **26**, 1825–1840 (2018).
29. Kues, M. et al. Quantum optical microcombs. *Nat. Photonics* **13**, 170–179 (2019).
30. Ma, Z. H. et al. Ultrabright quantum photon sources on chip. *Phys. Rev. Lett.* **125**, 263602 (2020).
31. Yin, Z. H. et al. Frequency correlated photon generation at telecom band using silicon nitride ring cavities. *Opt. Express* **29**, 4821–4829 (2021).
32. Lu, H. H. et al. Generation and characterization of ultrabroadband polarization–frequency hyperentangled photons. *Opt. Lett.* **48**, 6031–6034 (2023).
33. Lu, H. H. et al. Frequency-bin photonic quantum information. *Optica* **10**, 1655–1671 (2023).
34. Fan, Y. R. et al. Multi-wavelength quantum light sources on silicon nitride micro-ring chip. *Laser Photonics Rev.* **17**, 2300172 (2023).
35. Wen, W. J. et al. Polarization-entangled quantum frequency comb from a silicon nitride microring resonator. *Phys. Rev. Appl.* **20**, 064032 (2023).
36. Zeng, H. et al. Quantum light generation based on GaN microring toward fully on-chip source. *Phys. Rev. Lett.* **132**, 133603 (2024).
37. Fan, J., Dogariu, A. & Wang, L. J. Generation of correlated photon pairs in a microstructure fiber. *Opt. Lett.* **30**, 1530–1532 (2005).
38. Chen, J. et al. Fiber-based telecom-band degenerate-frequency source of entangled photon pairs. *Opt. Lett.* **31**, 2798–2800 (2006).
39. Fang, B. et al. State engineering of photon pairs produced through dual-pump spontaneous four-wave mixing. *Opt. Express* **21**, 2707–2717 (2013).
40. Reimer, C. et al. Cross-polarized photon-pair generation and bi-chromatically pumped optical parametric oscillation on a chip. *Nat. Commun.* **6**, 8236 (2015).
41. Zhang, Y. J. et al. Dual-pump approach to photon-pair generation: demonstration of enhanced characterization and engineering capabilities. *Opt. Express* **27**, 19050–19061 (2019).
42. Guo, Y. et al. Telecom-band degenerate-frequency photon pair generation in silicon microring cavities. *Opt. Lett.* **39**, 2526–2529 (2014).
43. Sabattoli, F. A. et al. Suppression of parasitic nonlinear processes in spontaneous four-wave mixing with linearly uncoupled resonators. *Phys. Rev. Lett.* **127**, 033901 (2021).
44. Lin, Q. & Agrawal, G. P. Silicon waveguides for creating quantum-correlated photon pairs. *Opt. Lett.* **31**, 3140–3142 (2006).
45. Sharping, J. E. et al. Generation of correlated photons in nanoscale silicon waveguides. *Opt. Express* **14**, 12388–12393 (2006).
46. Medic, M. et al. Fiber-based telecommunication-band source of degenerate entangled photons. *Opt. Lett.* **35**, 802–804 (2010).
47. Wu, J. P. et al. Multi-wavelength quantum light source with dual pumps. In: *Proceedings of 2023 Asia Communications and Photonics Conference/2023 International Photonics and Optoelectronics Meetings*. Wuhan: IEEE, 2023, 1–3.
48. Zhang, Y. B. et al. Induced photon correlations through the overlap of two four-wave mixing processes in integrated cavities. *Laser Photonics Rev.* **14**, 2000128 (2020).
49. Menotti, M. et al. Nonlinear coupling of linearly uncoupled resonators. *Phys. Rev. Lett.* **122**, 013904 (2019).
50. Franson, J. D. Bell inequality for position and time. *Phys. Rev. Lett.* **62**, 2205–2208 (1989).
51. Tittel, W. et al. Long-distance Bell-type tests using energy-time entangled photons. *Phys. Rev. A* **59**, 4150–4163 (1999).
52. Azzini, S. et al. From classical four-wave mixing to parametric fluorescence in silicon microring resonators. *Opt. Lett.* **37**, 3807–3809 (2012).
53. Dong, S. et al. True single-photon stimulated four-wave mixing. *ACS Photonics* **4**, 746–753 (2017).
54. Bennett, C. H., Brassard, G. & Mermin, N. D. Quantum cryptography without Bell's theorem. *Phys. Rev. Lett.* **68**, 557–559 (1992).
55. Gisin, N. et al. Quantum cryptography. *Rev. Mod. Phys.* **74**, 145 (2002).
56. Ma, X. F., Fung, C. H. F. & Lo, H. K. Quantum key distribution with entangled photon sources. *Phys. Rev. A* **76**, 012307 (2007).
57. Yin, J. et al. Satellite-to-ground entanglement-based quantum key distribution. *Phys. Rev. Lett.* **119**, 200501 (2017).
58. Yin, J. et al. Entanglement-based secure quantum cryptography over 1120 kilometres. *Nature* **582**, 501–505 (2020).
59. Pelet, Y. et al. Operational entanglement-based quantum key distribution over 50 km of field-deployed optical fibers. *Phys. Rev. Appl.* **20**, 044006 (2023).
60. Wu, C. et al. Bright photon-pair source based on a silicon dual-mach-zehnder microring. *Sci. China Phys. Mech. Astron.* **63**, 220362 (2020).
61. Chen, N. et al. Parity-time-symmetry-enabled broadband quantum frequency-comb generation. *Phys. Rev. A* **110**, 023714 (2024).
62. Lucas, E. et al. Tailoring microcombs with inverse-designed, meta-dispersion microresonators. *Nat. Photonics* **17**, 943–950 (2023).
63. Steiner, T. J. et al. Continuous entanglement distribution from an AlGaAs-on-insulator microcomb for quantum communications. *Opt. Quantum* **1**, 55–62 (2023).
64. Steiner, T. J. et al. Ultrabright entangled-photon-pair generation from an AlGaAs-on-insulator microring resonator. *PRX Quantum* **2**, 010337 (2021).
65. Pang, Y. M. et al. Versatile chip-scale platform for high-rate entanglement generation using an AlGaAs microresonator array. *PRX Quantum* **6**, 010338 (2025).